

BGA Joint Microstructure of Sn-Ag Based Solders with Au/Ni-P Plating

Keisuke Uenishi, Shigeaki Sakatani*, Takashi Yamamoto and Kojiro F. Kobayashi

Department of Manufacturing Science, Osaka University, 2-1 Yamadaoka, Suita, Osaka 565-0871, Japan

Fax: 81-6-6879-7570, e-mail: uenishi@mapse.eng.osaka-u.ac.jp

* Present Address Matsushita Electric Industrial Co., Ltd.

Fax: 81-6-6905-1537, e-mail: sakatani.shigeaki@jip.panasonic.com

The microstructure and strength for the BGA joint of Pb free Sn-Ag and Sn-Ag-Cu solder balls with Au/Ni-P plating were investigated by high resolution TEM observation. For the BGA joint using Sn-Ag solder, Ni₃Sn₄ reaction layer formed at the solder/pad interface and also P-rich layer formed in Ni-P plating. The P-rich layer was confirmed to be composed of the Ni-P-Sn ternary compound layer and crystallized Ni₃P layer. The spherical voids formed by Kirkendall effect were observed within the Ni-P-Sn ternary compound layer. Defects were also observed in the crystallized Ni₃P layer, but the morphology was spindly. Since the area surrounding these voids was hardly crystallized, these defects are assumed to be formed by the volume changes from amorphous to crystallized structure. Formation of these P rich layers lowered the joint strength. On the contrary, the alloying of Cu into solder changed the reaction layer to (Au, Cu, Ni)₆Sn₅ and such P rich layers were not formed. Between (Cu, Ni)₆Sn₅ layers and Ni-P plating, thin layer composed of Sn, Cu, Ni and P was observed by TEM observation, but it still retained the amorphous structure free from voids.

Key words: lead free solder, ball grid array, interfacial reaction, joint strength, joint microstructure

1. INTRODUCTION

Compared to more conventional packages, such as the pin through hole or the quad flat package, the ball grid array (BGA) packages have the advantages of having higher input/output terminal density, smaller footprint, and higher reliability [1]. In the BGA packaging, module chips and substrates are usually connected by using solder balls.

Recent environmental regulations against Sn-Pb solder require the development of substantial Pb free solders [2]. By the debt of the many researchers' efforts, several kinds of lead free solders have been selected as the candidate of substitutional solders. Especially, Sn-Ag based solders are recognized to have the most favorable properties among them. In estimating the applicability of lead free solders, it is important not only to investigate the property of the solder itself but also to examine the solderability with substrate. In this sense, since Sn-Ag solders have a higher melting temperature [3], it is important to control the interaction with substrates and to suppress the excessive growth of the reaction layer formed on the joint interface.

The authors have previously reported the solderability of Sn-Ag based solders with Au/Ni-P electroless plating which is usually coated on the substrate as an under bump metallurgy [4,5]. Compared with eutectic Sn-Pb solders, the reactivity of Sn-Ag based solders with the plating was enhanced due to the increased reflow soldering temperature. Moreover, the BGA joints using Sn-Ag solders were found to be less reliable due to the formation of so-called "P rich layer" on the joint interface. Although the small addition of Cu to the Sn-Ag solders was confirmed to solve this problem, it is not still clear about the reason why this P

rich layer was formed and why P rich layer degrade the joint reliability. Actually the phases composing the P rich layer has not identified yet.

In this research, in order to identify the P rich layer, the detailed microstructural observation of the reaction layer including the P rich layer was performed by using TEM and high resolution TEM study. Also the joint microstructure using Cu added Sn-Ag-Cu solders was observed by TEM. After discussing the mechanism for the interfacial structure formation, the reason why Cu addition is effective for controlling the reactivity with Au/Ni-P plating will be clarified. And then, effect of joint microstructure on the joint strength was discussed.

2. EXPERIMENTAL

The BGA substrates used in this experiment are the Cu pads on which surface 5 μm thick Ni-P and 0.04 μm thick Au were electroless plated. About 7mass% of P is contained in the Ni-P plating. As solder balls, for types of solder balls *i.e.* Sn-37mass%Pb, Sn-3.5mass%Ag, Sn-3.5mass%Ag-0.75mass%Cu and Sn-2mass%Ag-0.75mass%Cu-3mass%Bi were prepared. Diameter of balls was fixed to 760 μm. Figure 1 shows the schematic illustration of a solder ball and pad for the BGA joint used in this study.

For the BGA joining, solder balls were dipped into rosin flux and then planted on the pads manually. The samples were reflowed three times by using a hot air oven. The peak reflow temperature was 513K and reflow time for which solder balls melt was 90s. After the reflow, the BGA joints were subjected to additional heat exposure at an aging temperature 423K for the aging time ranging from 0.5h to 500h. To investigate the microstructural evolution of the joints, the cross-sections

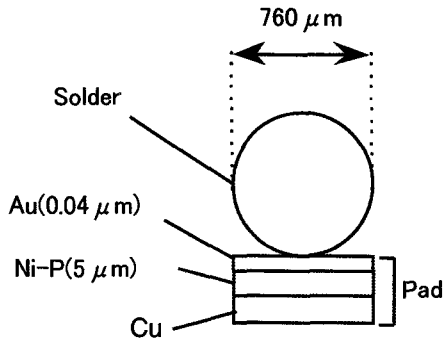


Fig.1 Schematic illustration of BGA joint used in this research

of the samples were observed by scanning electron microscopy (SEM) with energy dispersive X-ray (EDX) analyses.

For the transmission electron microscopy (TEM) observation, samples were thinned to the thickness of less than 100nm by irradiating the Ga ion with a focused ion beam milling (FIB) apparatus. For the compositional analysis of nano-order sized area, the sample was observed by the high resolution TEM.

For the estimating the mechanical properties of BGA joints, three types of tests i.e. shear test, cold bump pull test and hot bump pull test were performed by the bonding test apparatus (DAGE, DAGE-SERIES -4000P, DAGE-SERIES-2000PC). In the shear test, the shear tool was set 0.1mm distant from the substrate and the traverse speed was fixed to 0.2mm/s. Figure 2 shows the schematic illustration of cold bump pull test and hot bump pull test. In the pull test, the traverse speed was 0.3mm/s. The maximum load measured during mechanical tests was compared.

3. RESULTS AND DISCUSSION

3.1 Intermetallic layers formed on joint interface

Figure 3 shows the SEM microstructures adjacent to the bond interface for the BGA joints using Sn-Pb, Sn-Ag and Sn-Ag-Cu solders after reflow soldering at 513K.

Dispersion of needle shaped Ag_3Sn in a matrix Sn was observed for an as reflowed Sn-Ag solder, while eutectic structure composing of Sn and Pb was observed for Sn-Pb solders. By the addition of Cu, Cu_6Sn_5 (η') phase newly appeared although the volume fraction of η' was smaller than that of the other phases.

On the joint interface between solders and pads, the Au plating completely disappeared from the interface just after reflow, leaving the Ni-P layer exposed to the solder. On the interface between solders and Ni-P layer, formation of reaction layer was confirmed for all the joints. Table I shows the results of quantitative EDX analyses for the reaction layer. For the joints using Cu free solders, Ni and Sn based reaction layer was formed. By referring the composition of the reaction layer as shown in Table 1 to the binary Ni-Sn phase diagram, it is found that the molar ratio of Sn against that of Ni is 4:3 suggesting that the reaction layer is composed of Ni_3Sn_4 phase. For the joints using Cu bearing Sn-Ag-Cu or Sn-Ag-Cu-Bi solders, on the contrary, Au, Cu, Ni and Sn was detected in the reaction layer. The molar ratio of Sn against the sum of Cu, Au and Ni was 5:6 and the composition of Au increased near solder while that of Ni increased near the Ni-P plating. These results suggest that the reaction layer is Cu-Sn based η' - $(\text{Au, Cu, Ni})_6\text{Sn}_5$ phase. The complete solid solubility of Au in η' - Cu_6Sn_5 phase has already confirmed in the ternary Au-Cu-Sn phase diagram [6].

In comparison of BGA joints using Cu bearing

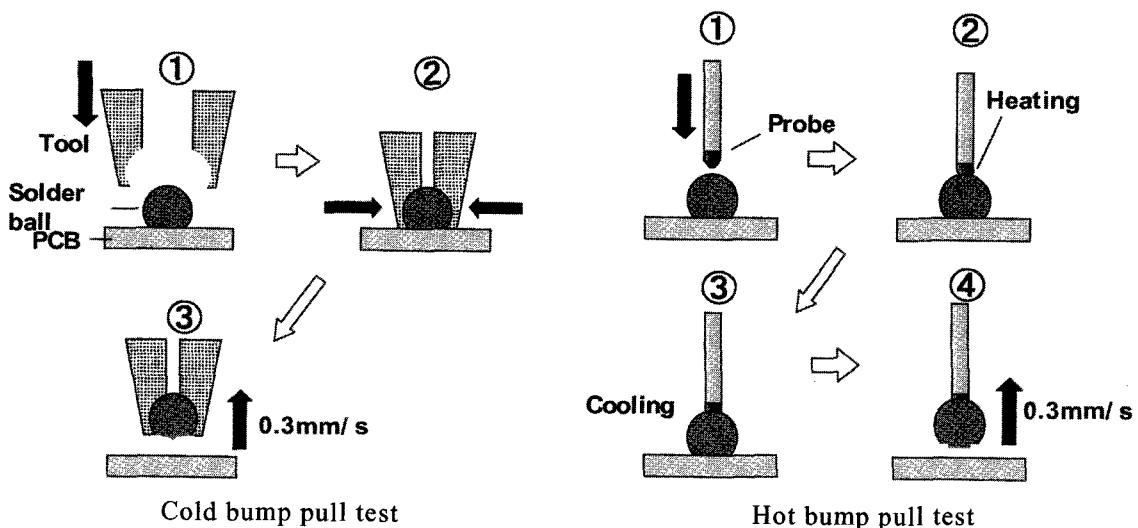


Fig. 2 Schematic illustration of cold bump pull test and hot bump pull test

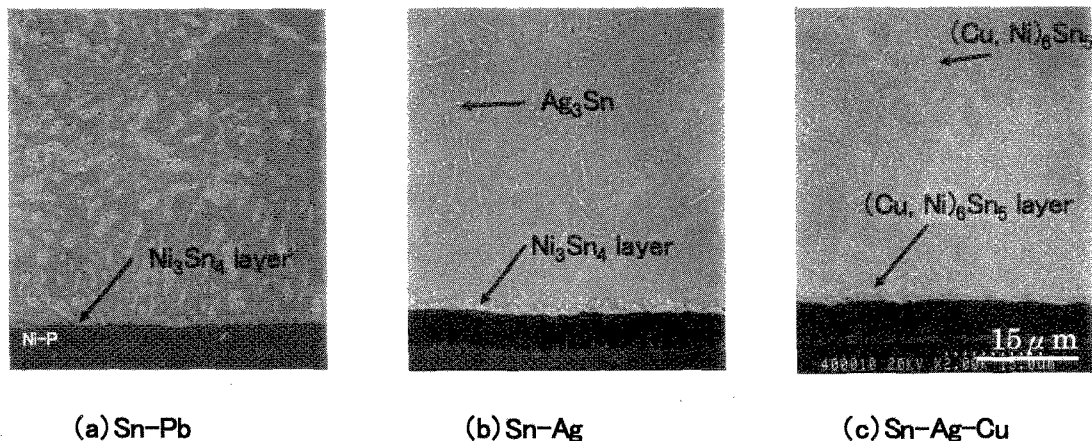


Fig.3 SEM images of BGA joint microstructure using (a)Sn-Pb, (b)Sn-Ag and (c) Sn-Ag-Cu solders

Table I Results of EDX compositional analyses of the reaction layers

	Sn	Ni	Cu	Au
Sn-Ag	55.8	42.1	-	0.2
Sn-Ag-Cu	44.2	18.6	36.6	0.4

(mol%)

solders with those using Cu free solders, it was confirmed that the reaction layers changed from the Ni-Sn based intermetallic phases to Cu-Sn based phases by Cu alloying into the solders. Moreover, on the boundary between Ni_3Sn_4 reaction layer and Ni-P plating for the joints using Cu free solders, the formation of a thin layer with a thickness of less than $1\ \mu\text{m}$ was confirmed. This reaction layer contains larger molar fraction of P than that of the as received Ni-P plating and is so-called P rich layer. Alloying of 3mass% Bi hardly affected the interfacial reaction and Bi was solid solved in Sn.

3.2 TEM observation of P rich layers

Figure 4 shows the TEM image for the microstructure around the P rich layer formed on the interface between Ni_3Sn_4 reaction layer and Ni-P plating. As shown in Fig.4, the P rich layer was recognized to be composed of two layers. Table 2 shows the chemical composition of each layer measured by EDX analyses. These layers were certainly richer in P than the as received Ni-P plating. While the upper layer was composed of three elements, Sn, Ni and P while the lower layer was composed of Ni and P. The analyzed chemical composition was almost constant within the upper layer. Thus the upper layer was supposed to be composed of the $\text{Ni}_6\text{Sn}_3\text{P}$ ternary intermetallic compound although any electron diffraction analyses could not be performed due to the lack of diffraction data. Meanwhile, the lower layer was considered to be composed of the Ni_3P compound and the amorphous Ni-P with lower concentration of P from the chemical compositional analyses. Actually, the electron

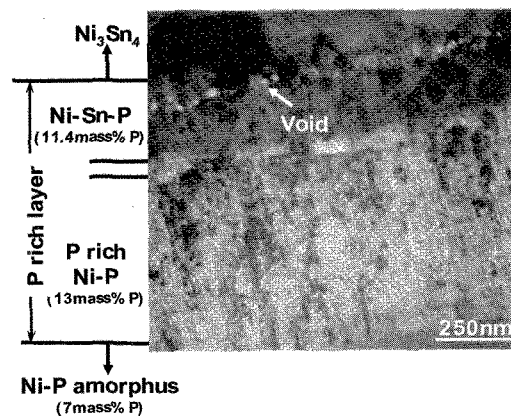


Fig.4 TEM image around the P rich layer formed on the interface between Ni_3Sn_4 reaction layer and Ni-P plating for the micro joint using Sn-Ag solder

diffraction pattern coming from this layer corresponded well with that of Ni_3P phase.

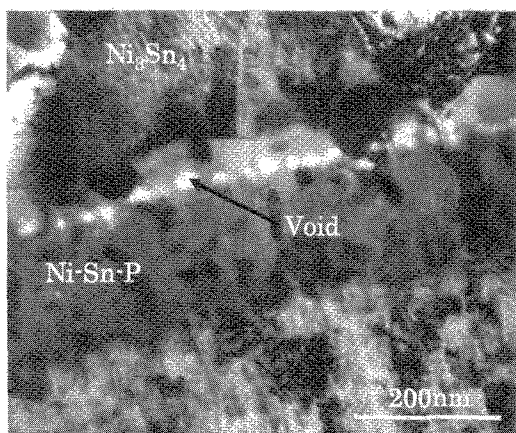
Figure 5 shows the microstructure of these P rich layers observed by higher magnification. The grain morphology in these layers was so different that the Ni-Sn-P layer exhibited the nearly equiaxed nano structure while the Ni_3P grains had the large aspect ratio. These morphologies of each grain are related to the formation mechanism of the layers. Namely, the upper Ni-Sn-P layer was formed through the interdiffusion between Sn-Ag solder and Ni-P plating. On the contrary, P rich Ni-P layer was formed by the one way diffusion of Ni from Ni-P plating toward the solders to form Ni_3Sn_4 intermetallic layer. As received Ni-P plating was almost composed of amorphous phase. It is generally known that the amorphous phase becomes less stable by increasing the molar fraction of P. Thus, when Ni diffuses from Ni-P plating toward the solder, the amorphous Ni-P plating crystallizes to the Ni_3P and the nucleated Ni_3P grain grows preferentially toward solders. Kariya et al. has confirmed the good relation in the reaction layer growth kinetics between Ni_3Sn_4 layer

and Ni₃P layer during heat exposure [7].

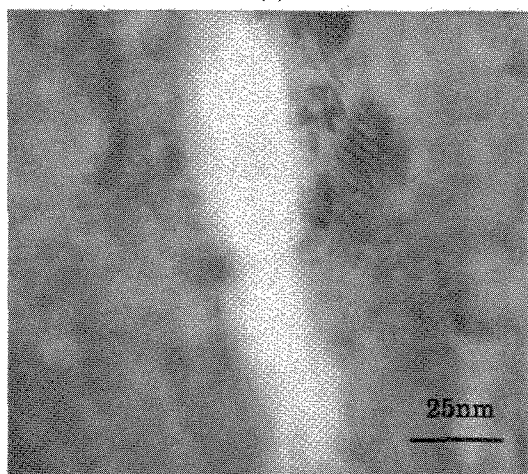
As shown in Fig.5, these two P rich layers were observed to include defects. The fine spherical voids were observed to line up in a row to the parallel direction of bondline, while the defects observed in Ni₃P layers were spindly. Judging from the morphology of voids, the voids in Ni-Sn-P layers was considered to be formed by Kirkendall effect. On the contrary, the area surrounding the spindly voids in P rich Ni-P layer was confirmed to have almost the same composition as Ni-P plating and to be hardly crystallized. Since it is generally known that the crystallization of the Ni-P amorphous phase decreases its volume, these defects are assumed to be formed by the volume changes from amorphous to crystallized structure.

3.3 TEM observation of joint interface using Sn-Ag-Cu solder

Figure 6 shows the TEM image for the interface between η' -Cu₆Sn₅ reaction layer and Ni-P plating. Not like the BGA joint using Sn-Ag solders, the thickness of intermediate was extremely small. Table 2 shows the chemical composition of this intermediate layer. Although it is suspicious if the signal was obtained only from the layer, Ni, Sn, Cu and P were



(a)



(b)

Fig.5 TEM micrograph of (a) Sn-Ni-P layer and (b) defects in the Ni₃P layer observed for the micro joints using Sn-Ag solder

confirmed to diffuse in this layer. However, the amount of diffusion is small and the composition of this layer was almost same as that of Ni-P plating. Consequently, this intermediate layer still retained the amorphous structure.

3.4 Strength of BGA joints and the relation to the microstructure

Figure 7 shows the changes in shear fracture load, cold bump pull fracture load and hot bump pull fracture load for the BGA joints using various solders. For all of the solders, the fracture load varied by the testing methods. Among three tests examined in this research, the cold bump pull test exhibited the highest fracture load and the shear test showed the lowest fracture load. This difference in the fracture load is deeply related to the fracture mode of the sample. Namely, in the shear test with the lowest fracture load, fracture occurred in the solders for all of the samples. On the contrary, in the cold or hot bump pull test, the fracture occurred mainly in the joint interface. In this sense, the bump pull test rather than the shear test is the suitable method to estimate the joint strength within the condition range performed in this research [8].

When the fracture load of the joints was compared for the hot bump pull test, it is noticed that the application of Sn-Ag solder decreased the joint strength. This is due to the existence of P rich layer. As shown in 3.3, the P rich layer is composed of the more brittle phases. Besides, the P rich layer contains many defects. Although the P rich layer was formed by using the

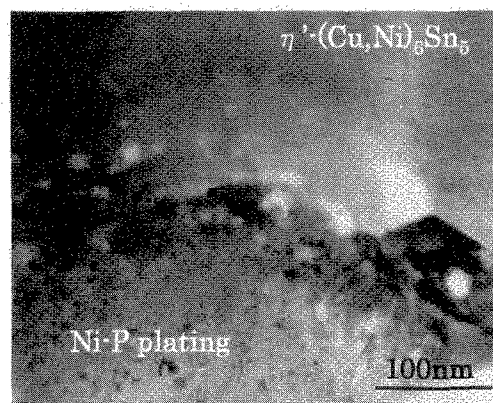


Fig. 6 TEM image of the interface between η' -Cu₆Sn₅ reaction layer and Ni-P plating for the micro joint using Sn-Ag-Cu solder

Table II Results of EDX compositional analyses of the intermediate reaction layers

	Ni	Sn	Cu	P
Intermediate layer	68.1	11.3	7.0	11.6

(mol%)

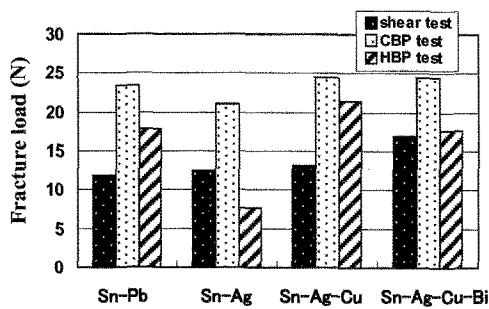


Fig.7 Changes in shear fracture load, cold bump pull fracture load and hot bump pull fracture load for the BGA joints using various solders

Sn-Pb solders, the thickness of the P rich layer is larger for the Sn-Ag solders due to the larger volume fraction of Sn and to the higher melting temperature. In comparison with BGA joints using Cu free solders, the joints using Cu bearing solders exhibited the higher joint strength because of the absence of P rich layers. P rich layers were formed by the interfacial reaction of Ni with Sn, but the Cu alloying into the solders changed the reaction layer to the Cu-Sn based compounds, which plays an important role as a barrier layer to suppress the Ni-Sn reaction. Suppress the reaction layer growth for the joints using Pb free solders.

4. CONCLUSION

The microstructure and strength for the BGA joint of Pb free Sn-Ag and Sn-Ag-Cu solder balls with Au/Ni-P plating were investigated by HRTEM observation. The main results obtained in this research are summarized as follows.

- (1) Alloying of Cu into Pb-Sn or Sn-Ag solders changed the intermetallic compound reaction layer Ni_3Sn_4 to Cu-Sn based η' - $(\text{Cu}, \text{Ni})_6\text{Sn}_5$.
- (2) For the BGA joints using Cu free solders, a P-rich layer formed between Ni_3Sn_4 and Ni-P plating. The P-rich layer was confirmed to be composed of Ni-P-Sn ternary compound layer and crystallized Ni_3P layer. The thickness of these P-rich layers had the proportional relation to that of Ni_3Sn_4 layer, which grows during heat exposure at 423K.
- (3) The spherical voids were observed in the center of the Ni-P-Sn ternary compound layer probably due to the diffusion between solders and plating. Spindly defects were also observed in the crystallized Ni_3P layer. Since the area surrounding these defects was hardly crystallized, these defects are assumed to be formed by the volume changes from amorphous to crystallized structure.
- (4) For the joints using Cu bearing solders, any rich layer was hardly formed. Although formation of very thin intermediate reaction layer composed of Cu, Ni, Sn and P was confirmed between $(\text{Cu}, \text{Ni})_6\text{Sn}_5$ reaction

layer and Ni-P plating, it still retained the amorphous structure free from voids.

- (5) Among three tests examined in this research, the cold bump pull test exhibited the highest fracture load and the shear test showed the lowest fracture load. This difference in the fracture load is deeply related to the fracture mode of the sample. Namely, in the shear test with the lowest fracture load, fracture occurred in the solders for all of the samples. On the contrary, in the cold or hot bump pull test, the fracture occurred mainly in the joint interface. In this sense, the bump pull test rather than the shear test is the suitable method to estimate the joint strength.
- (6) When the fracture load of the joints was compared for the hot bump pull test, it is noticed that the application of Sn-Ag solder remarkably decreased the joint pull strength due to the existence of P rich layer, which is composed of brittle Ni_3P and many defects.

ACKNOWLEDGEMENT

The authors thank Prof. H. Mori and Dr. J. Lee, Research Center for Ultra-High Voltage Electron Microscopy in Osaka University, for the experimental help and giving us the useful suggestion about the high resolution TEM study. This research is financially supported by JSPS grant –in aid for Scientific Research.

REFERENCES

- [1] J. S. Kaper and J. S. Prener, *Acta Crystallogr.*, **7**, 246-48 (1954).
- [2] F. Izumi, "The Rietveld Method", Ed. by R. A. Young, Oxford University press, Oxford (1993) pp. 121-24.
- [1] E. Bradley and K. Banerji, *IEEE Trans. Comp. Pkg. & Mfg. Technol.*, **B.18**, 320-31 (1996).
- [2] A.M.Minor and J.W.Morris, Jr. *J. Electron. Mater.*, **29**, 1170-74 (2000).
- [3] S.K.Kang, R.S.Rai and S.Purushothaman, *J. Electron. Mater.* **25**, 1113-20 (1996)
- [4] K.Uenishi, T.Saeki, Y.Kohara, K.F.Kobayashi, I. Shoji, M.Nishiura and M.Yamamoto, *Mater. Trans.*, **42**, 756-60 (2001)
- [5] K.Uenishi, Y.Kohara, S.Sakatani, K.F. Kobayashi and M.Yamamoto, *Mater. Trans.*, **43**, 1833-39 (2002)
- [6] J.F.Roeder, M.R.Notis and J.I.Goldstein: *Defect and Diffusion Forum*, **59** (1988), 271-278.
- [7] Y.Kariya, private communication
- [8] M.Nishiura, A.Nakayama, S.Sakatani, Y.Kohara, T.Saeki, K.Uenishi and K.F. Kobayashi, *Mater. Trans.*, **43**, 1802-07 (2002)

(Received October 10, 2003; Accepted October 31, 2003)